Renewable Energy 211 (2023) 31–41

Contents lists available at ScienceDirect

Renewable Energy

journal homepage: www.elsevier.com/locate/renene

# pH-depended behaviors of electrolytes in nanofluidic salinity gradient energy harvesting

Xi Chen [a], Lu Wang [a], Ruhong Zhou [b], Rui Long [a,*], Zhichun Liu [a], Wei Liu [a]

[a] School of Energy and Power Engineering, Huazhong University of Science and Technology, Wuhan, 430074, PR China
[b] School of Mechanical Science and Engineering, Huazhong University of Science and Technology, Wuhan, 430074, PR China

ARTICLE INFO

*Keywords:*
Nanofluidic reverse electrodialysis
pH
Electrolytes
Machine learning

ABSTRACT

Transmembrane ion transportation in the nanofluidic salinity gradient energy conversion process is significantly regulated by the ion characteristics and concentration-depended physical and chemical properties of the electrolyte solution. In this paper, considering the Born and dielectrophoretic forces and nonhomogeneous electrolyte solution, impacts of various electrolytes on the nanofluidic energy conversion performance are systematically investigated under various solution pHs. When the solution pH is less than the isoelectric point (IEP), with $BeCl_2$ solution employed, where the anion diffusion and concentration coefficient are much larger than those of the anion, significant transmembrane anion diffusion exists, leading to the highest osmotic current and maximum power output, even when the solution pH > IEP where the nanochannel is negatively charged, the ion selectivity is still not altered. At pH < IEP, 2:1 electrolytes, where the cation has small ion diffusion coefficient and the anion has larger diffusion coefficient and hydrated radius could result in upgraded energy conversion performance; At pH > IEP, 1:1 electrolytes where the cation has large ion diffusion coefficient and the anion has small diffusion coefficient and large hydrated radius are more appealing. In addition, the relationships between ion characteristics, power extracted, and energy conversion efficiency are further obtained via machine learning.

## 1. Introduction

Widespread utilization of traditional fossil energy sources has induced severe environmental pollution problems and climate issues. Exploiting green and renewable energy sources has received increasing attention [1]. Salt gradient power (SGP) is considered a promising green energy source with large magnitudes. The SGP originates from the concentration potential difference generated by mixing brines with different concentrations [2,3]. Reverse electrodialysis (RED) is considered an efficient method to utilize the SGP, which separates concentrated and dilute solutions through alternating CEMs and AEMs [4] and can be combined with other systems such as low-grade waste heat [5,6]. And the directional movement of the ions through the IEMs generates an ionic current. The electrodes of both ends of the membrane stack transfer the ionic current into the electrical current, converting the salt gradient energy into useable electrical energy [7–9].

Constrained by the sub-nano pores of the IEMS, the power densities in traditional IEMs typically are usually below 10 $W/m^2$ [10–12]. To mitigate such issues in traditional RED process, nanofluidic reverse electrodialysis was developed to offer a high SGP conversion performance [13]. In the nanofluidic reverse electrodialysis, charged nanopores which repel co-ions and attract counter ions can function as the IEMs. The power density via boron nitride nanochannels reached 4 $kW/m^2$, of which the magnitude of the currents was two orders higher than the traditional RED device [14]. Feng et al. [15] developed a monolayer $MOS_2$ film composed of novel $MoS_2$ material and obtained an energy density of $10^6$ $W/m^2$.

The performance of macro- and nanofluidic reverse electrodialysis is mainly impacted by membrane properties, temperature, ion concentration, geometry, and ionic species [7,16–19]. Tseng et al. [20] investigated the effects of temperature and nanopore size on NREDs and revealed that larger temperature results in higher power density, and longer and smaller sized channels conbribute to ion selectivity. He et al. [21] designed three-dimensional nanochannels using poly ionic liquids materials that reduced the path of ion motion as well as providing abundant surface charge density and achieved a maximum power output

* Corresponding author. School of Energy and Power Engineering, Huazhong University of Science and Technology, Wuhan, 430074, PR China.
*E-mail addresses:* cx413@hust.edu.cn (X. Chen), l_wang@hust.edu.cn (L. Wang), 1317832173@qq.com (R. Zhou), r_long@hust.edu.cn (R. Long), zcliu@hust.edu.cn (Z. Liu), w_liu@hust.edu.cn (W. Liu).

https://doi.org/10.1016/j.renene.2023.04.056
Received 30 May 2022; Received in revised form 1 April 2023; Accepted 13 April 2023
Available online 26 April 2023

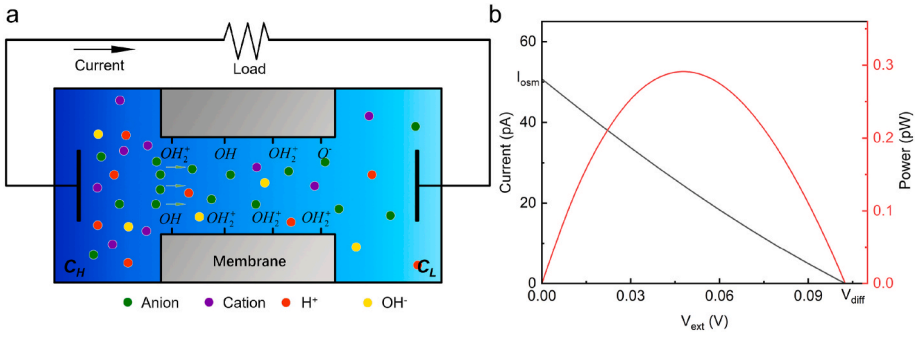


**Fig. 1.** (a) Schematic diagram of salinity gradient energy conversion process, (b) I–V curves of the salinity gradient energy conversion process, where 100 mM KCl and 1 mM KCl are emplpoyed at the nanochannel ends, respectively.

of 4.33 W/m$^2$ by mixing the artificial seawater and river water. Ren et al. [22] used a designed interfacial nanostructures to improve ion selectivity. Zhang et al. [23] employed the oxidation of black phosphorus (BP) to improve the efficiency of osmotic energy conversion, and the power density was increased by 220% to 1.6 W/m$^2$ compared with the original BP film. Zhang et al. [24] obtained a power density of 4.1 W/m$^2$ during the mixing of artificial river water and seawater via a nanofiber composite membrane, and found that the coupling of the surface charge of MXene with the space charge generated by the nanofibers played a key role in the ion diffusion process. Two-dimensional nanosheets have also been used to harvest salinity gradient energy, as they could provide higher ion fluxes and larger osmotic currents [25,26]. Long et al. [27] proposed three synergy angles to describe the relationship between the ion diffusion and the electrostatic migration driven forces, and employed a nanowire blocker inserted in the nanopore to enhance the energy conversion performance. Graf et al. [28] modified the electronic structure of $MoS_2$ surface by light irradiation, and achieved a 130% increase in power output at pH close to neutral conditions. Wang et al. [29] investigated the interfacial effects induced by temperature and ion concentration at the molecular dynamics level and found that elevated temperature and low concentration contribute to effective ion diffusion and selectivity. Zhang et al. [30] incorporated a photothermal conversion structure into the salinity gradient utilization component, which enabled conversion of solar energy to heat the solution that improved ion diffusion coefficient and fluid convection. In addition, Long et al. [31] systematically investigated the energy conversion performance with transmembrane temperature difference involved, and the synergy between the concentration gradient and temperature gradient was revealed. To step further, the criteria for selecting membranes based on the thermal conductivity were proposed in non-isothermal operation conditions [32].

The ion types also present a significant effect on the salinity gradient energy conversion process [33]. The presence of divalent ions in most cases presents a negative effect on the energy acquisition process, as the voltage generated by multivalent ions is lower than that of monovalent ions. To balance the voltage in the membrane stack, a portion of the voltage generated by monovalent ions is used to transport the multivalent ions from low to high concentrations, called uphill transport phenomenon. The uphill transport leads to a significant decrease in the voltage performance of the solution when monovalent and divalent ions are mixed [34]. Vermaas et al. [34] investigated the performance of multivalent ions represented by magnesium sulfate when mixed with NaCl solution and found that magnesium ions and sulfate have important effects on open-circuit voltage and power density. Rijnaarts et al. [35] studied the performance of divalent cations in REDs, which can reduce the power density, demonstrating that the use of new commercial cation exchange membranes can mitigate these effects by allowing only monovalent ions to pass through. Pintossi et al. [36] found the mixing of multivalent ions leads to a 25% decrease in power density. Post et al. [37] showed that multivalent ions in dilute solutions have a more obvious reduction effect on the voltage of a membrane stack. The flux of divalent ions in the mixed solution can be reduced by employing the IEMs that allow only monovalent ions to pass through. Güler et al. [38] employed coatings to improve the selectivity for monovalent ions. Abdollahzadeh et al. [39] designed a new IEM with angstrom-scale asymmetric MOF-on-MOF cavities, which contributes to the selectivity of monovalent ions in mixed solutions. However, the use of multivalent permeation membranes in solutions with high magnesium ion concentrations is more efficient in the long term [40]. Pintossi et al. [41] improved the numerical model for predicting the membrane resistance, conductivity, and power density of the RED in the presence of sulfate and magnesium ions.

As the salinity gradient energy harvesting is significantly impacted by the electrolytes involved, previous studies are mainly focused on the specific monovalent, divalent ions or their mixtures. The selection criteria for desired electrolytes rendering upgraded performance has been never reported with the solution pH considered. In this paper, considering the Born and dielectrophoretic forces acting on the ions and the nonhomogeneous electrolyte solution characterized by concentration-depended permittivity and viscosity, the impacts of electrolytes whose anions and cations described by the hydrated radius and valence and diffusion coefficient on the nanofluidic energy conversion performance are systematically investigated via the ion selectivity, ionic current, membrane potential, maximum power output and the corresponding energy conversion efficiency. Machine learning is further employed to reveal the relationships between ion characteristics (hydrated radius and valence and diffusion coefficient), power extracted and energy conversion efficiency. The selection criteria for desired electrolytes at various pHs have been developed, and some meaningful conclusions have been drawn.

## 2. Methods

As shown in Fig. 1, we consider a cylindrical nanochannel of radius $R_n = 8$ nm, length $L_n = 500$ nm, which connects two solution reservoirs of radius $R_r = 800$ nm, length $L_r = 800$ nm filled with aqueous electrolyte solution at a concentration of 500 mM and 1 mM, respectively. Here, the nanochannel is assumed to be made of track-etched polyethylene terephthalate (PET), which carries the functional carboxyl groups AH and B. At the nanochannel/liquid interface, following dissociation reactions exist: AH<=>$A^-$ + $H^+$ and $BH^+$≤>B+$H^+$. The reaction equilibrium constants in above reactions are defined as $K_A = [A^-][H^+]/[AH]$ and $K_B = [B][H^+]/[BH^+]$. The spatially distributed surface charge density on the nanochannel wall can be described by Ref. [42]:

$$\sigma_W = -\left(10^{18} e N_{\text{total}}\right)\left\{\frac{10^{-pK_A} - 10^{-pK_B}\left([H^+]_S\right)^2}{10^{-pK_A} + 10^{-pK_B}\left([H^+]_S\right)^2 + [H^+]_S}\right\} \quad (1)$$

where $pK_A = -\log(K_A)$, $pK_B = -\log(K_B)$, $[H^+]_S$ is the $H^+$ concentration

at the nanochannel/liquid interface. $e$ is the elementary charge. $N_{\text{total}}$ is the total density of the functional groups. For the PET membrane, $pK_A = 2.302$, $pK_B = 9.453$ at $T = 298K$ [43]. The isoelectric point (IEP) is about 6.

According to Ref. [44], the viscosity and permittivity of a solution in the nanochannel are impacted by the volume occupied by ions. Considering the Born and dielectrophoretic forces acting on the ions and the nonhomogeneous electrolyte solution characterized by concentration-depended permittivity and viscosity, the modified Nernst−Planck-Poisson equations are employed to describe the transmembrane ion transportation characteristics in the salinity gradient energy conversion process [45,46].

The modified Navier−Stokes equation is written as [46,47].

$$\begin{aligned}&-\eta(\vec{r})\nabla\times\nabla\times\vec{v}(\vec{r})+\nabla\eta(\vec{r})\cdot[\nabla\vec{v}(\vec{r})+\nabla\vec{v}^{\mathrm{T}}(\vec{r})]\\&=\nabla P(\vec{r})+\rho_s[\vec{v}(\vec{r})\cdot\nabla]\vec{v}(\vec{r})+eN_{\mathrm{A}}\sum_{i=1}^{m}z_ic_i(\vec{r})\nabla\Psi(\vec{r})\end{aligned}\tag{2}$$

where $N_A$ is the Avogadro number, and $\eta$ is the viscosity of the electrolyte solution.

The continuity equation for the electrolyte solution is

$$\nabla\cdot\vec{v}(\vec{r})=0\tag{3}$$

The Poisson equation is

$$\nabla[\varepsilon(\vec{r})\nabla\Psi(\vec{r})]=-eN_{\mathrm{A}}\sum_{i=1}^{m}z_ic_i(\vec{r})\tag{4}$$

The conservation equation for the ions is

$$\nabla\cdot\left[\vec{J}_i(\vec{r})\right]=0\tag{5}$$

where the ionic flux $\vec{J}_i$ is [47]

$$\begin{aligned}\vec{J}_i(\vec{r})&=c_i(\vec{r})\vec{v}_i(\vec{r})\\&=-D_i(\vec{r})\nabla c_i(\vec{r})-\frac{ez_iD_i(\vec{r})c_i(\vec{r})}{kT}\nabla\Psi(\vec{r})+c_i(\vec{r})\vec{v}(\vec{r})\\&\quad-D_i(\vec{r})c_i(\vec{r})\nabla\ln\gamma_i(\vec{r})-\frac{z_i^2e^2D_i(\vec{r})c_i(\vec{r})}{8\pi kTR_i}\nabla\left[\frac{1}{\varepsilon(\vec{r})}\right]\\&\quad+\frac{2\pi\varepsilon(\vec{r})R_i^3D_i(\vec{r})c_i(\vec{r})}{kT}\frac{\varepsilon_i-\varepsilon(\vec{r})}{\varepsilon_i+2\varepsilon(\vec{r})}\nabla E^2(\vec{r})\end{aligned}\tag{6}$$

where $c_i$, $v_i$, $\gamma_i$, and $D_i$ are the local concentration, velocity, activity coefficient, and diffusion coefficient of the $i$-th ionic species. $R_i$ is the hydrated radius. The local electric field is denoted as $E$; $v$ and $\varepsilon$ are the local velocity and permittivity of the solution. $k$ is the Boltzmann constant. The local activity coefficient for the $i$-th ionic specie is described by [48,49]

$$\begin{aligned}\ln\gamma_i(\vec{r})=&-\left(1-12R_i^2\frac{\xi_2^2}{\xi_3^2}+16R_i^3\frac{\xi_2^3}{\xi_3^3}\right)\ln(1-\xi_3)\\&+\frac{2R_i\left(3\xi_2+6R_i\xi_1+4R_i^2\xi_0\right)}{1-\xi_3}\\&+\frac{12R_i^2\xi_2(\xi_2+2R_i\xi_1\xi_3)}{\xi_3(1-\xi_3)^2}\\&-\frac{8R_i^3\xi_2^3\left(\xi_3^2-5\xi_3+2\right)}{\xi_3^2(1-\xi_3)^3}\end{aligned}\tag{7}$$

where $\xi_j(\vec{r})=\frac{2^{j-1}\pi N_{\mathrm{A}}}{3}\sum_{i=1}^{m}c_i(\vec{r})R_i^j\quad j\in\{0,1,2,3\}$.

The permittivity of the electrolyte solution is calculated by

$$\begin{aligned}\frac{\varepsilon(\vec{r})-\varepsilon_s}{\varepsilon(\vec{r})+2\varepsilon_s}&=\sum_{i=1}^{m}\varphi_i(\vec{r})\frac{\varepsilon_i-\varepsilon_s}{\varepsilon_i+2\varepsilon_s}\\&=\frac{4}{3}\pi N_{\mathrm{A}}\sum_{i=1}^{m}R_i^3c_i(\vec{r})\frac{\varepsilon_i-\varepsilon_s}{\varepsilon_i+2\varepsilon_s}\end{aligned}\tag{8}$$

**Table 1**
Grid independence validation.

| Grid number | 87,800 | 129,000 | 195,000 | 288,000 |
|---|---|---|---|---|
| Osmotic Current | −177.11 | −177.29 | −177.6 | −177.71 |
| Relative errors | 0.33% | 0.23% | 0.06% | – |

where $\varphi_i=\frac{4\pi R_i^3}{3}N_Ac_i$ is the local volume fraction of the $i$-th ionic specie.

The viscosity of the electrolyte solution is given by

$$\eta(\vec{r})=\eta_s\left[1+2.5\varphi(\vec{r})+5.2\varphi(\vec{r})^2\right]\tag{9}$$

where the total volume fraction $\varphi$ is

$$\varphi(\vec{r})=\sum_{i=1}^{m}\varphi_i(\vec{r})=\frac{4\pi}{3}N_{\mathrm{A}}\sum_{i=1}^{m}R_i^3c_i(\vec{r})\tag{10}$$

The concentration depended on diffusion coefficient is given by

$$D_i(\vec{r})=\frac{\eta_s}{\eta(\vec{r})}D_i^{\infty}\tag{11}$$

where $D_i^{\infty}$ is the diffusion coefficient of the ions at infinite dilution.

The interior surface of the nanochannel is assumed to have a pH-depended surface charge density of $\sigma_W$ with no ion flux $\mathbf{J}_i$. The electrolyte concentration at the reservoirs is fixed at 500 mM and 1 mM, respectively. No external pressure gradient is applied across the reservoirs. The electrical potential at the end of the low concentration and high concentration reservoir is respectively set to $V_{ext}$ and 0. $-\varepsilon\mathbf{n}\cdot\nabla\varphi=0$ on $\Omega_r$ and $\Lambda_j$, $\mathbf{n}\cdot\mathbf{J}_i=0$ on $\Omega_r$ and $\Lambda_j$, $-\varepsilon\mathbf{n}\cdot\nabla\varphi=\sigma$ on $\Omega_n$, where $\Omega_n$, $\Omega_r$, $\Lambda_j$ denote the boundaries at the channel surface, the inner surface of the reservoir, and the reservoir ends, respectively.

The ionic current is calculated as $I=\int_A F(\sum_i^4 z_iJ_i)\cdot nd\Lambda$. The nanochannel presents different selectivity for cations or anions depending on the solution pHs. The ion transference number is defined as

$$t=\left|\frac{|I_+|-|I_-|}{|I_+|+|I_-|}\right|\tag{12}$$

where $I_+$ and $I_-$ are the ionic current contributed by cations and anions. $t=0$ means the nanochannel presents no selectivity for cations or anions. $t=1$ indicates the nanochannel exhibits ideal selectivity for cations or anions. As shown in Fig. 1, for the $I$–$V$ curves of the energy conversion process, the ionic current presents a nearly linear relationship with various applied voltages. Therefore, the membrane potential (open-circuit voltage, $E_{mem}$) can be calculated by linear interpolation via the ionic currents under different applied voltages. The osmotic current (short circuit current, $I_{osm}$) is obtained with no external voltage applied. The maximum power output is calculated as $P_{max}=E_{mem}\,I_{osm}/4$. The energy conversion efficiency under the maximum power output can be further written as $\eta_p=t^2/2$.

## 3. Results and discussion

### 3.1. Model validation

The numerical equations are solved with the Multiphysics software COMSOL, where the calculation domain is meshed with quadrilateral elements, and finned meshes are applied near the nanochannel walls. The calculation is first conducted via different mesh numbers, which vary exponentially, thus to guarantee the calculated results are mesh-independent. The results of grid independence validaton are shown in Table 1. The difference of the osmotic current between the grid number of 195,000 and 288,000 is less than 0.1%. Therefore the grid number of 195,000 is used for following calculation in present study.

The model employed is then validated by the calculated results and the experimental ones in Ref. [14]. The boron nitride nanochannel is

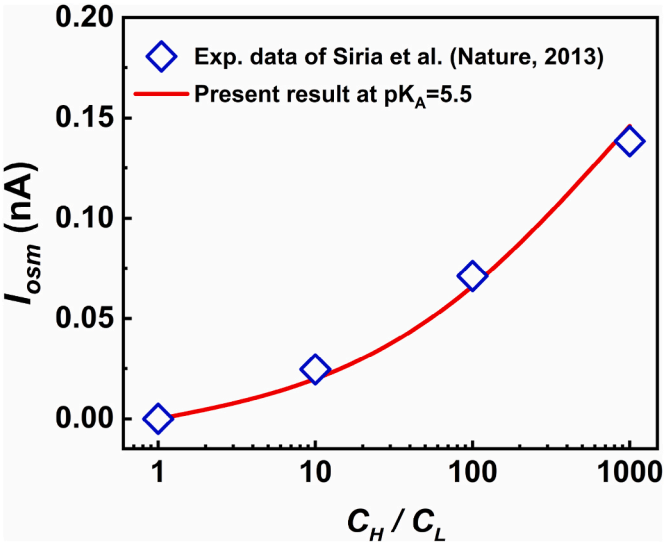


**Fig. 2.** Comparisons between the calculated results and the experimental ones from Ref. [14]. In the calculation, $N_{total}$ is fixed at 7 sites/nm$^2$ in accord with those in previous literature (about 6–18 sites/nm$^2$) [14,50].

**Table 2**
Diffusion coefficients and hydrated radius of the selected anions and cations.

| Ion species | Diffusion coefficient ($m^2\ s^{-1}$) | Hydrated radius (nm) | Ion species | Diffusion coefficient ($m^2\ s^{-1}$) | Hydrated radius (nm) |
|---|---|---|---|---|---|
| $Li^+$ | 1.030 | 0.382 | $Na^+$ | 1.330 | 0.358 |
| $K^+$ | 1.960 | 0.331 | $Rb^+$ | 2.110 | 0.329 |
| $Cs^+$ | 2.060 | 0.329 | $Ba^{2+}$ | 0.848 | 0.404 |
| $Be^{2+}$ | 0.599 | 0.459 | $Ca^{2+}$ | 0.793 | 0.412 |
| $H^+$ | 9.31 | 0.282 | $OH^-$ | 5.27 | 0.3 |
| $Cl^-$ | 2.030 | 0.332 | $Br^-$ | 2.010 | 0.330 |
| $I^-$ | 2.045 | 0.300 | $MnO_4^-$ | 1.632 | 0.345 |
| $ClO_4^-$ | 1.792 | 0.338 | $NO_3^-$ | 1.900 | 0.335 |

1250 nm long and its radius is 40 nm. The KCl concentration at the low concentration side is set at 1 mM. The transmembrane concentration ratio varies from 1:1 to 1000:1. The solution pH is fixed at 5.5. As shown in Fig. 2, the calculated osmotic currents match well with the experimental ones, thus the employed numerical model is justified.

### 3.2. Maximum power under various electrolytes and pHs

The selected anions and cations in the present study are listed in Table 2. To guarantee satisfied solubility of the aqueous electrolyte solutions, monovalent and divalent cations are involved while the anions are monovalent. The diffusion coefficients and hydrated radius of the selected anions and cations are listed in Table 2. According to the chemical valence of the cations and anions, the electrolytes are classified into two groups, namely 1:1 electrolytes and 2:1 electrolytes. The pH of the electrolyte solutions varies from 3 to 9 with the isoelectric point (IEP) at pH = 6.

As shown in Fig. 3, in the studied pH values, the highest maximum power output occurs at pH = 3. When pH < IEP, such as pH = 3 and pH = 5, the 2:1 electrolytes present higher maximum power output than the 1:1 electrolytes. When pH > IEP, such as pH = 7 and pH = 9, the 1:1 electrolytes present higher maximum power output than the 2:1 electrolytes. The electrolytes rendering the top three larger maximum power output under various pHs are presented in Fig. 4. For 1:1 electrolytes, the maximum power output first decreases, achieves its minimum values at pH = IEP = 6, then increases. When pH < IEP, LiCl renders the largest maximum power output, followed by LiBr and LiI. When pH > IEP, $RbMnO_4$ leads to the largest maximum power output. And CsMnO4 presents the second-largest maximum power output. For 2:1 electrolytes, anomalous phenomenon exists. $BeCl_2$ presents the largest maximum power output. The maximum power output first decreases obviously, then slightly decreases with increasing pHs. In the studied 1:1 and 2:1 electrolytes, when pH < IEP, $BeCl_2$ presents the largest maximum power output. At pH = 3, the maximum power output under $BeCl_2$ solution is nearly twice as that under LiCl solution. When pH > IEP, $RbMnO_4$ exhibits the largest maximum power output.

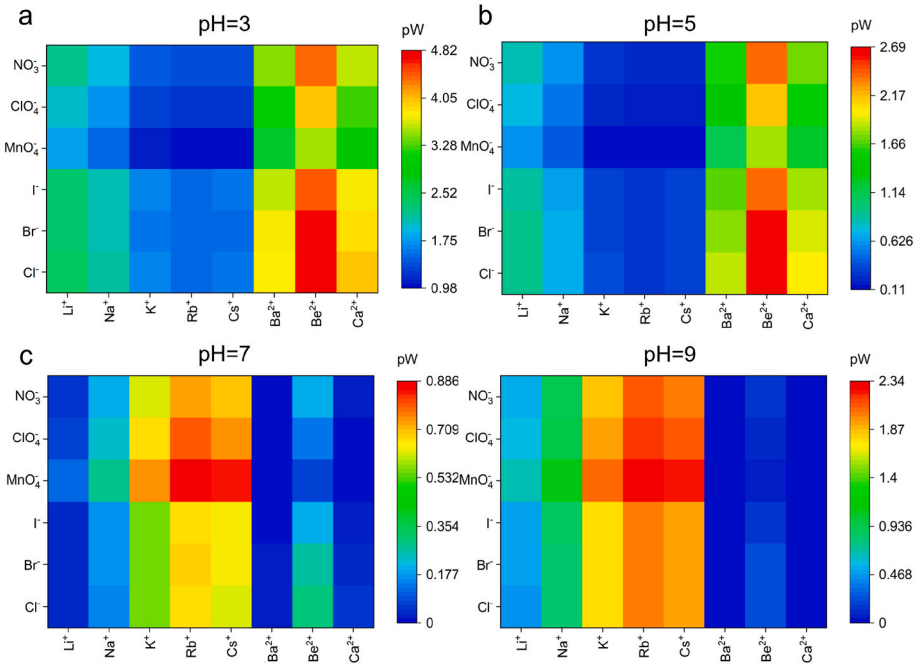


**Fig. 3.** Maximum power output under various electrolytes and solution pHs.

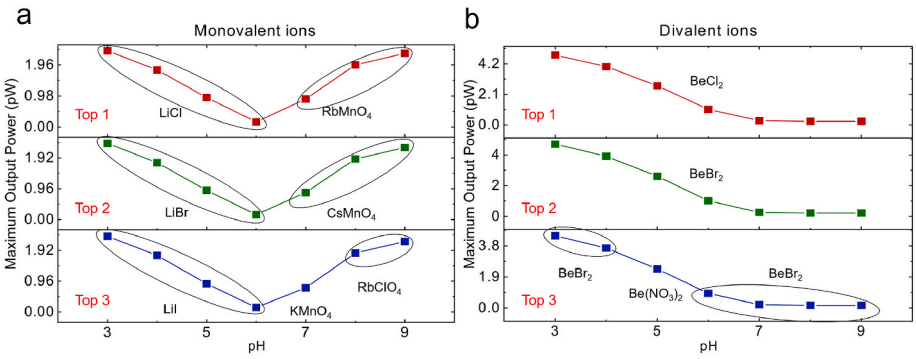


**Fig. 4.** Top three electrolytes with respect to maximum power output under various solution pHs for 1:1 electrolytes and 2:1 electrolytes.

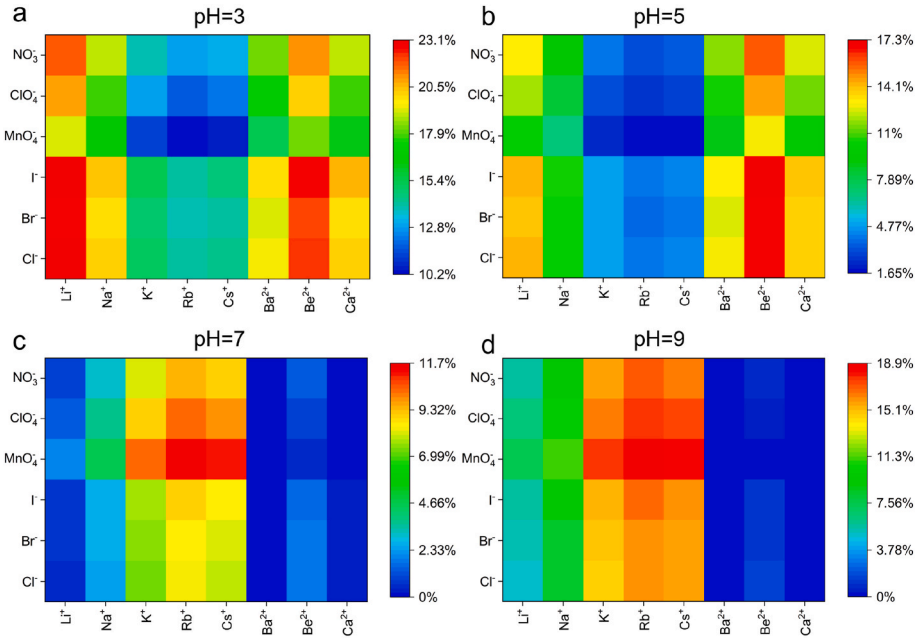


**Fig. 5.** Energy conversion efficiency at maximum power output under various electrolytes and solution pHs.

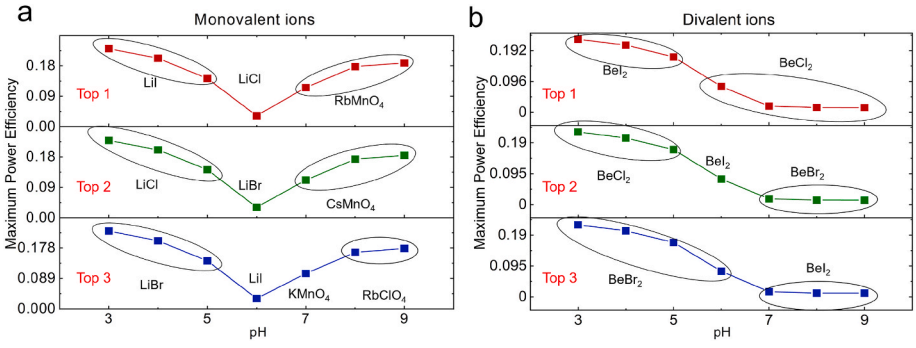


**Fig. 6.** Top three electrolytes with respect to energy conversion efficiency at maximum power output under various solution pHs for 1:1 electrolytes and 2:1 electrolytes.

### *3.3. Energy conversion efficiency at maximum power under various electrolytes and pHs*

As shown in Fig. 5, when pH < IEP, the electrolytes with cations of $Li^+$, $Na^+$,$Ba^{2+}$, $Be^{2+}$, $Ca^{2+}$ lead to larger energy conversion efficiency at maximum power output than the others. When pH > IEP, an opposite phenomenon exists. The electrolytes with cations of $K^+$, $Rb^+$, $Cs^+$ result in larger energy conversion efficiency at maximum power output. As shown in Fig. 6, when the solution pH is far away from the IEP, for 1:1 electrolytes at pH = 3, the electrolytes leading to the first three energy conversion efficiency are LiI, LiCl, and LiBr. When pH = 9, the electrolytes leading to the top three energy conversion efficiency are $RbMnO_4$, $CsMnO_4$, and $RbClO_4$. The energy conversion efficiency at pH = 3 is larger than that at pH = 9. For 2:1 electrolytes, the energy

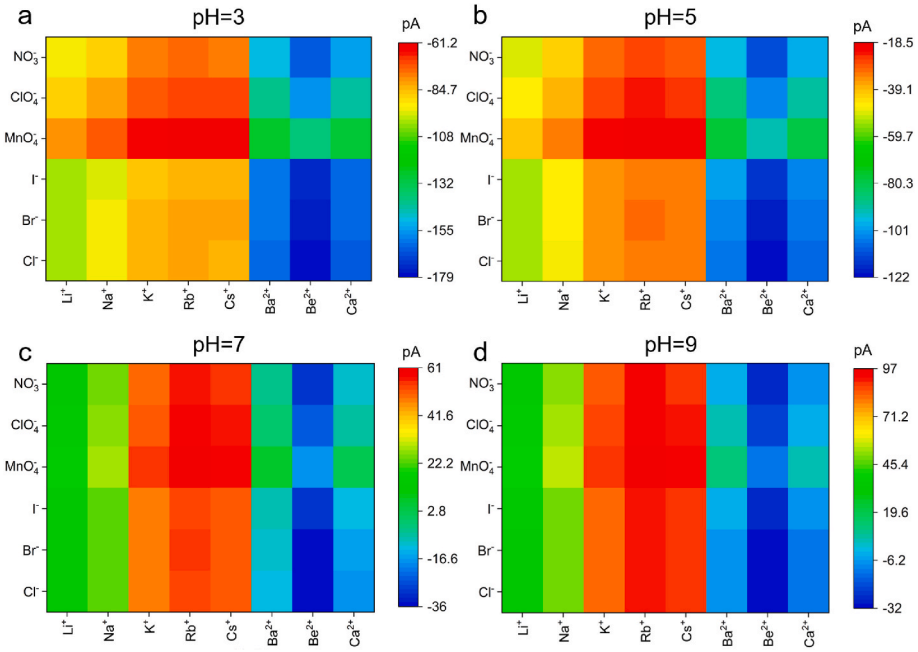


**Fig. 7.** Osmotic current under various electrolytes and solution pHs.

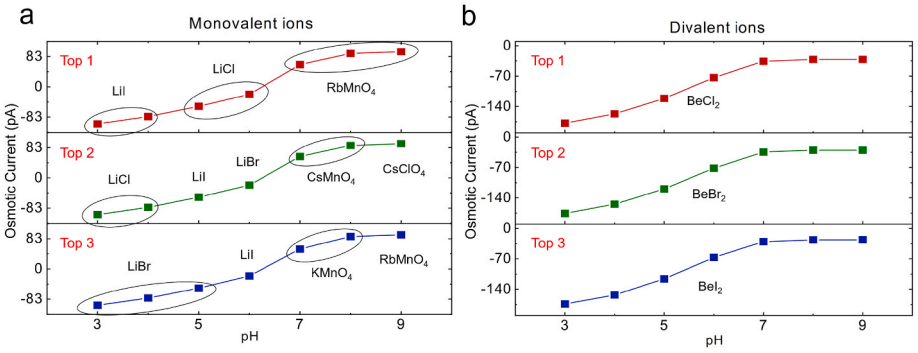


**Fig. 8.** Top three electrolytes with respect to osmotic current under various solution pHs for 1:1 electrolytes and 2:1 electrolytes.

conversion efficiency decreases with increasing pHs. At pH = 3, the electrolytes leading to the first three energy efficiency are $BeI_2$, $BeCl_2$, and $BeBr_2$. When pH = 9, the electrolytes leading to the first three energy efficiency are $BeCl_2$, $BeBr_2$, and $BeI_2$.

### 3.4. Osmotic current under various electrolytes and pHs

As shown in Fig. 7, when pH < IEP, the osmotic current of the 2:1 electrolytes is much larger than that of the 1:1 electrolytes, as the nanochannel is positively charged, which presents the selectivity for the anions. The anion concentration of the 2:1 electrolytes is much larger than that of the 1:1 electrolytes, leading to a much higher osmotic current. Due to higher surface charge density at lower solution pHs, which contribute to the EDL overlapping degree and charge separation. The osmotic current at pH = 3 is much larger than that at pH = 5. When the solution pH > IEP, the nanochannel wall is negatively charged, which attracts cations and repels anions, exhibiting selectivity for cations. The osmotic current changes its sign for 1:1 electrolytes. However, for some 2:1 electrolytes such as $BeCl_2$, the selectivity is not altered. It originates from the fact that the diffusion coefficient of $Be^{2+}$ is much less than that of $Cl^-$ and the concentration of $Cl^-$ is much higher than $Be^{2+}$, although the nanochannel has the selectivity for cations, the transmembrane $Cl^-$ diffusion is too significant, leading to more $Cl^-$ passing through the nanochannel. At larger pHs, the negative surface charge density is augmented, therefore for 1:1 electrolytes, the osmotic current increases with increasing solution pHs. For some 2:1 electrolytes, such as $BeCl_2$, larger surface charge density increases the EDL overlapping degree, which facilitates $Be^{2+}$ passing by and hinders $Cl^-$, the osmotic current decreases. The top three electrolytes with respect to the osmotic current are depicted in Fig. 8. For 1:1 electrolytes, when pH < IEP, LiI renders the largest osmotic current, as $Li^+$ has the smallest diffusion coefficient and $I^-$ has the largest diffusion coefficient among the studied ions. The nanochannel at pH < IEP presents the selectivity for anions. Large anion diffusion coefficient and small cation diffusion coefficient induce a higher osmotic current. At pH > IEP, $RbMO_4$ renders the largest osmotic current, as $Rb^+$ has the largest diffusion coefficient and $MnO_4^-$ has a relatively small diffusion coefficient and largest hydrated radius that induces significant steric and dielectric forces, which hinders $MnO_4^-$ passing by. For 2:1 electrolytes, $BeCl_2$ renders the largest osmotic current, as $Be^{2+}$ has the smallest diffusion coefficient and $Cl^-$ has the relatively large diffusion coefficient and hydrated radius among the studied ions.

### 3.5. Ion selectivity under various electrolytes and pHs

As the nanochannel presents different selectivity for ions at various

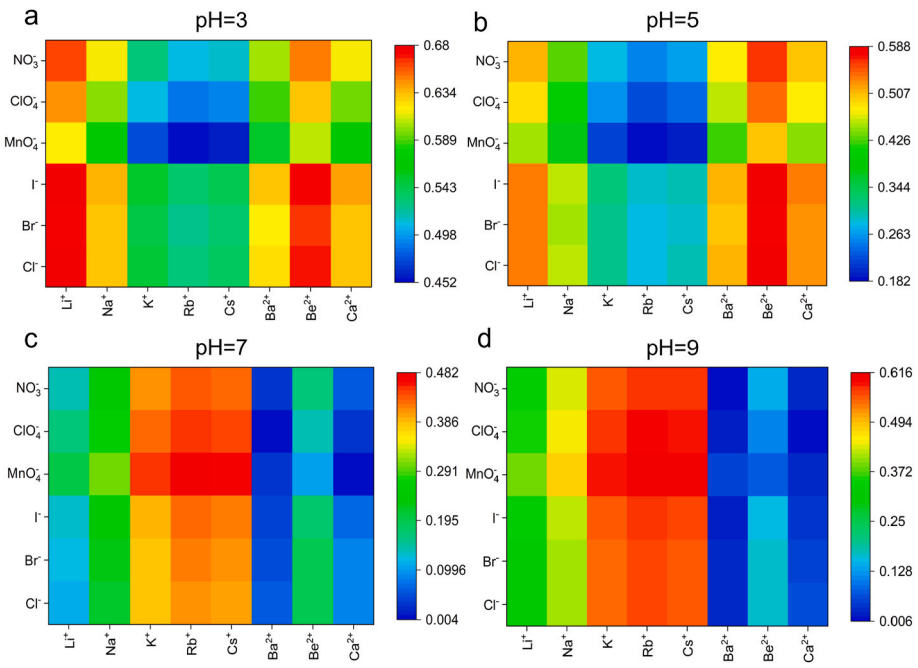


**Fig. 9.** Ion selectivity under various electrolytes and solution pHs.

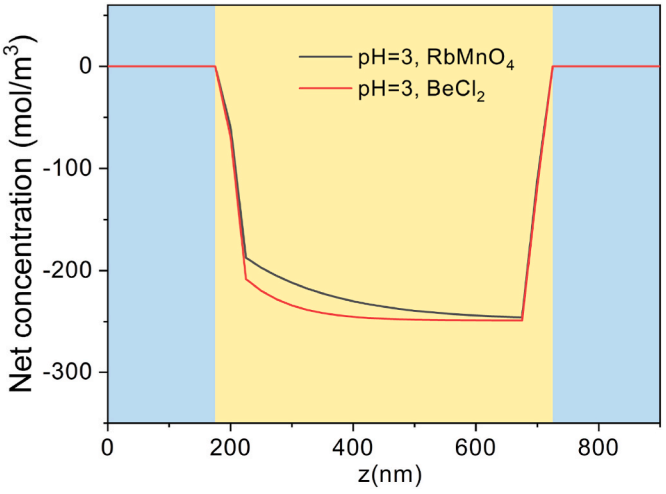


**Fig. 10.** Axial cross-sectionally net ion concentration under various electrolytes at pH = 3.

pHs. The ion transference number is defined as $t = (|I_+| - |I_-|)/(|I_+| + |I_-|)$ $t = 0$ means the nanochannel presents no ion selectivity. A larger $t$ means higher ion selectivity for cations or anions. When pH < IEP, the nanochannel wall is positively charged, which attracts anions and repels cations, presenting anion selectivity. When pH > IEP, the nanochannel wall is negatively charged, which attracts cations and repels anions, presenting cation selectivity. As shown in Fig. 9, when pH < IEP, the electrolytes with cations of $Li^+$, $Na^+$, $Ba^{2+}$, $Be^{2+}$, $Ca^{2+}$ render larger transference numbers than the others. When pH > IEP, an opposite phenomenon exists. The electrolytes with cations of $K^+$, $Rb^+$, $Cs^+$ leads to larger transference numbers. To step further, the net and average cross-sectional ion concentration is calculated

$$C_{net} = \frac{\int_0^{R_n} \left[\sum_{i=1}^{4} z_i C_i\right] \cdot 2\pi r dr}{\pi {R_n}^2} \tag{13}$$

$$C_{ave} = \frac{\int_0^{R_n} \left[\sum_{i=1}^{4} |z_i C_i|\right] \cdot 2\pi r dr}{\pi {R_n}^2} \tag{14}$$

As shown in Fig. 10, When pH < IEP such as pH = 3, the net cross-sectional ion concentration of $BeCl_2$ in the nanochannel interior is much large than that of $RbMO_4$, indicating more significant effects of the EDL overlapping degree and improved ion separation, therefore larger ion selectivity. In the salinity gradient energy conversion processes, significant ion concentration polariton exists, especially at the low concentration end where the ion concentration differs from the bulk one, as shown in Fig. 11. When the pH is far away from the IEP, the pH-depended surface charge density increases, which contributes to the EDL overlapping and the ion concentration polarization. The average cross-sectional ion concentration at pH = 3 is larger than that at pH = 5, meanwhile the average cross-sectional ion concentration at pH = 9 is larger than that at pH = 7. When pH < IEP, the average cross-sectional ion centration increases at the low concentration end with decreasing solution pH, which leads to decreased effective concentration ratio, as depicted in Fig. 11. (d). When pH > IEP, the average cross-sectional ion concentration at the low concentration end increases with increasing solution pH, leading to decreased effective concentration ratio.

### 3.6. Membrane potential under various electrolytes and pHs

The sign of the membrane potential at various pHs is the same as the osmotic current due to the pH-depended ion transportation regulated by the surface charge density and ion properties as aforementioned before. As shown in Fig. 12, for 1:1 electrolytes, the direction of the membrane potential is altered as the pH changes from pH<IEP to pH>IEP. For some 2:1 electrolytes, the direction of the membrane potential stays stable as the pH changes from pH<IEP to pH>IEP. As the membrane potential is determined by the transmembrane effective concentration ratio and transference number, for 1:1 electrolytes, LiCl renders the largest membrane potential when pH < IEP while $RbMO_4$ renders the largest one when pH > IEP. For 2:1 electrolytes, $BeCl_2$ always induces the largest membrane potential whether pH > IEP or pH < IEP in the studied pHs, as depicted in Fig. 13.

As the power output is calculated as $P_{max} = E_{mem}\ I_{osm}/4$. For 1:1

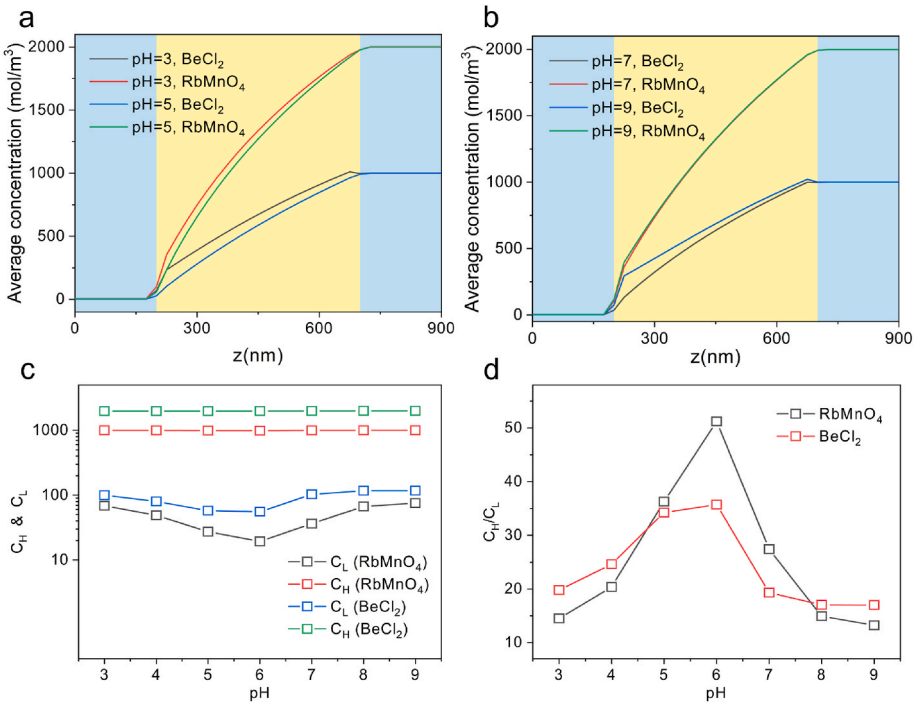


**Fig. 11.** (a,b) Axial cross-sectionally averaged ion concentration under various electrolytes and solution pHs; (c) cross-sectionally averaged ion concentration at the nanochannel ends; (d) effective transmembrane concentration ratio.

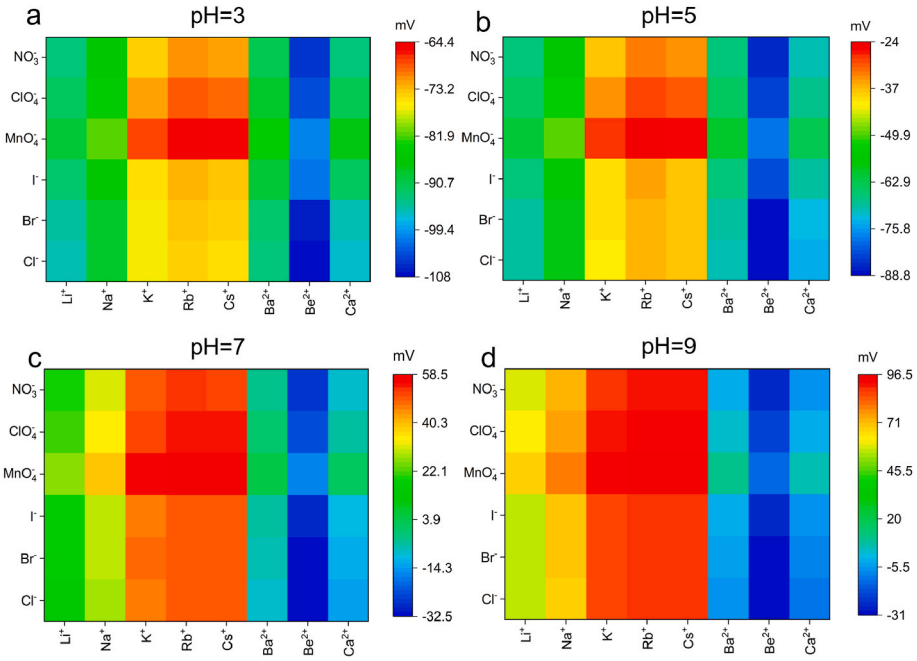


**Fig. 12.** Membrane potential under various electrolytes and solution pHs.

electrolytes, at pH < IEP, LiCl results in the largest membrane potential and second largest osmotic current, and the former is more significant, thus to achieve the highest power output. When pH > IEP, $RbMO_4$ leads to the largest osmotic membrane potential and osmotic current, thus the highest power output. For 2:1 electrolytes, $BeCl_2$ always leads to the largest osmotic membrane potential and osmotic current, thus the highest power output, as shown in Fig. 4. Overall, when pH < IEP, $BeCl_2$ has the largest power output in both the 1:1 and 2:1 electrolytes; When pH > IEP, $RbMnO_4$ presents the largest one. Therefore, at pH < IEP, 2:1 electrolytes, where the cation has small ion diffusion coefficient and the anion has larger diffusion coefficient and hydrated radius could result in upgraded energy conversion performance; At pH > IEP, 1:1 electrolytes where the cation has large ion diffusion coefficient and the anion has small diffusion coefficient and large hydrated radius are more appealing.

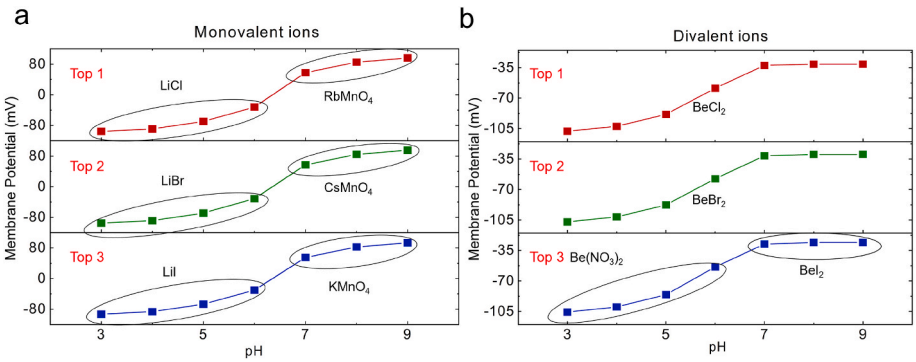


**Fig. 13.** Top three electrolytes with respect to membrane potential under various solution pHs for 1:1 electrolytes and 2:1 electrolytes.

**Table 3**
Indicators of machine learning models.

| Target objective | Method | RMSE | $R^2$ | MSE | MAE |
|---|---|---|---|---|---|
| Power | Ensembles | 0.0389 | 1 | 1.514e-3 | 2.21e-2 |
| | Decision Trees | 0.2129 | 0.96 | 4.53e-2 | 0.1262 |
| Efficiency | Ensembles | 9.85e-3 | 0.98 | 9.71e-5 | 7.20e-3 |
| | Decision Trees | 0.0124 | 0.97 | 1.543e-4 | 0.0089 |

## 4. Relationship between electrolyte properties and energy conversion performance via machine learning

Here machine learning is employed to reveal the relationship between electrolyte properties and energy conversion performance. The maximum power output $P_{max}$ and the corresponding energy conversion efficiency $\eta$ are considered as target variables and electrolyte properties (cation hydration radius $R_1$, cation diffusion coefficient $D_1$, cation valence $Z_1$, anion hydration radius $R_2$, anion diffusion coefficient $D_2$, and anion valence $Z_2$) are applied as feature variables. Two machine learning regression models are considered, namely ensembles and decision tree, which are widely used in analyzing energy conversion systems [27]. In the machine learning process, the hyperparameters of the models are optimized by the Bayesian optimization. Each training process is conducted several times to alleviate the random error. Root Mean Square Error (RMSE), Correlation coefficient ($R^2$), Mean Square Error (MSE), and Mean Absolute Error (MAE) are employed to evaluate the accuracy of the involved machine learning models. As shown in Table 3, regarding to the machine learning for the maximum power output, the $R^2$ based on the ensemble machine learning model is 1, which is higher than that based on the decision tree machine learning model. Regarding to the machine learning for the energy conversion efficiency corresponding to the maximum power output, the $R^2$ based on the ensemble and decision tree machine learning model 0.98 and 0.97 respectively, demonstration satisfied fitting accuracy, as illustrated in Fig. 14. Based on the constructed relationship, the energy conversion performance indicators under any given electrolyzes can be directly obtained, which can significantly save the computational resources and time costs of the computational fluid dynamics. Furthermore, via the constructed relationship, optimizations could further be conducted to obtain the optimal electrolyze characteristics under different objectives, which could offer as a guidance for designing and synthesizing electrolyzes that render satisfied energy conversion performance.

## 5. Conclusions

In this paper, considering the Born and dielectrophoretic forces

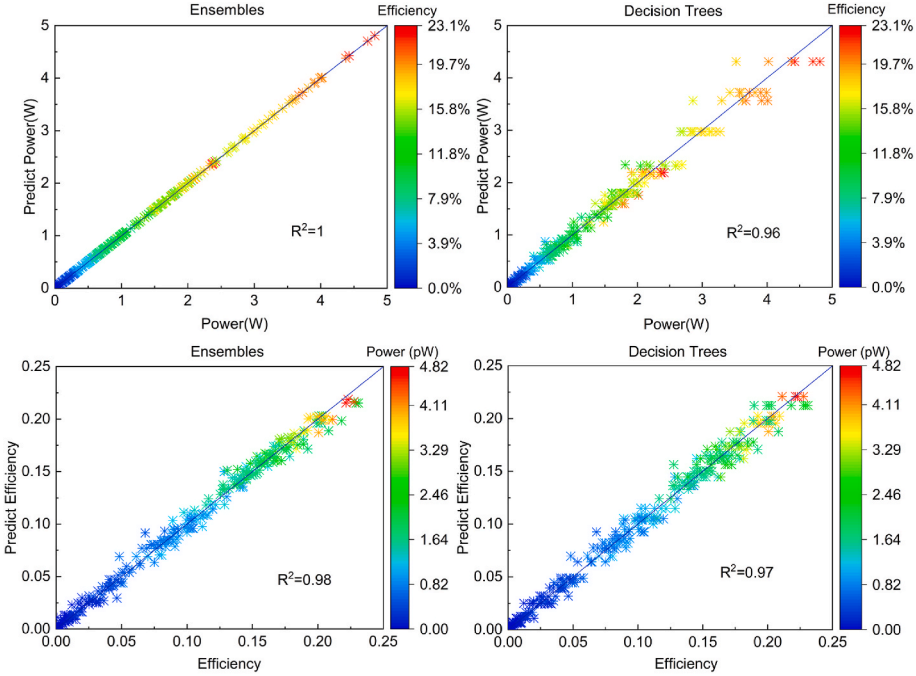


**Fig. 14.** Actual-predicted diagrams of maximum power output and maximum power efficiency via machine learning.

acting on the ions and the nonhomogeneous electrolyte solution characterized by concentration depended permittivity and viscosity, the impacts of electrolytes whose anions and cations characterized by the hydrated radius and valence and diffusion coefficient on the nanofluidic energy conversion performance are systematically investigated in the nanochannel with the length of 500 nm and radius of 8 nm under various solution pHs The main conclusions are drawn below.

(1) For 1:1 electrolytes, the osmotic current and membrane potential change their direction as the solution pH varies from pH<IEP to pH>IEP.
(2) For 2:1 electrolytes, such as $BeCl_2$, where the ion diffusion coefficient of $Be^{2+}$ is much less than that of $Cl^-$ and the concentration of $Cl^-$ is much higher than $Be^{2+}$, significant transmembrane $Cl^-$ diffusion exists, even when the solution pH > IEP where the nanochannel is positively charged, the ion selectivity is still not altered.
(3) At pH < IEP, 2:1 electrolytes, where the cation has small ion diffusion coefficient and the anion has larger diffusion coefficient and hydrated radius could result in upgraded energy conversion performance;
(4) At pH > IEP, 1:1 electrolytes where the cation has large ion diffusion coefficient and the anion has small diffusion coefficient and large hydrated radius are more appealing.
(5) The relationships between ion characteristics, power extracted and energy conversion efficiency are obtained via the machine learning.

## CRediT authorship contribution statement

**Xi Chen:** Writing – original draft, Visualization. **Lu Wang:** Formal analysis. **Ruhong Zhou:** Visualization. **Rui Long:** Methodology, Writing – review & editing, Funding acquisition. **Zhichun Liu:** Conceptualization. **Wei Liu:** Formal analysis.

## Declaration of competing interest

The authors declare that they have no known competing financial interests or personal relationships that could have appeared to influence the work reported in this paper

## Acknowledgements

This work is financially supported by the National Natural Science Foundation of China (52176070).

## References

[1] Z.-Q. Li, Z.-Q. Wu, X.-L. Ding, M.-Y. Wu, X.-H. Xia, A solar thermoelectric nanofluidic device for solar thermal energy harvesting, CCS Chemistry 3 (2021) 2174–2182.
[2] T. Rijnaarts, J. Moreno, M. Saakes, W.M. de Vos, K. Nijmeijer, Role of anion exchange membrane fouling in reverse electrodialysis using natural feed waters, Colloids Surf. A Physicochem. Eng. Asp. 560 (2019) 198–204.
[3] D.A. Vermaas, Energy Generation from Mixing Salt Water and Fresh Water: Smart Flow Strategies for Reverse Electrodialysis, 2014.
[4] F. Giacalone, P. Catrini, A. Tamburini, A. Cipollina, A. Piacentino, G. Micale, Exergy analysis of reverse electrodialysis, Energy Convers. Manag. 164 (2018) 588–602.
[5] K. Kwon, B.H. Park, D.H. Kim, D. Kim, Parametric study of reverse electrodialysis using ammonium bicarbonate solution for low-grade waste heat recovery, Energy Convers. Manag. 103 (2015) 104–110.
[6] J. Li, C. Zhang, Z. Wang, Z. Bai, X. Kong, Salinity gradient energy harvested from thermal desalination for power production by reverse electrodialysis, Energy Convers. Manag. 252 (2022), 115043.
[7] R. Long, Z. Kuang, Z. Liu, W. Liu, Reverse electrodialysis in bilayer nanochannels: salinity gradient-driven power generation, Phys. Chem. Chem. Phys. 20 (2018) 7295–7302.
[8] D. Pandey, S. Bhattacharyya, Impact of surface hydrophobicity and ion steric effects on the electroosmotic flow and ion selectivity of a conical nanopore, Appl. Math. Model. 94 (2021) 721–736.
[9] S. Pawlowski, R.M. Huertas, C.F. Galinha, J.G. Crespo, S. Velizarov, On operation of reverse electrodialysis (RED) and membrane capacitive deionisation (MCDI) with natural saline streams: a critical review, Desalination 476 (2020), 114183.
[10] D.A. Vermaas, M. Saakes, K. Nijmeijer, Doubled power density from salinity gradients at reduced intermembrane distance, Environ. Sci. Technol. 45 (2011) 7089–7095.
[11] J. Gao, W. Guo, D. Feng, H. Wang, D. Zhao, L. Jiang, High-performance ionic diode membrane for salinity gradient power generation, J. Am. Chem. Soc. 136 (2014) 12265–12272.
[12] B.D. Kang, H.J. Kim, M.G. Lee, D.-K. Kim, Numerical study on energy harvesting from concentration gradient by reverse electrodialysis in anodic alumina nanopores, Energy 86 (2015) 525–538.
[13] P. Cheng, S. Chen, X. Li, Y. Xu, F. Xu, A.J. Ragauskas, Tree-inspired lignin microrods-based composite heterogeneous nanochannels for ion transport and osmotic energy harvesting, Energy Convers. Manag. 255 (2022), 115321.
[14] A. Siria, P. Poncharal, A.-L. Biance, R. Fulcrand, X. Blase, S.T. Purcell, et al., Giant osmotic energy conversion measured in a single transmembrane boron nitride nanotube, Nature 494 (2013) 455–458.
[15] J. Feng, M. Graf, K. Liu, D. Ovchinnikov, D. Dumcenco, M. Heiranian, et al., Single-layer MoS 2 nanopores as nanopower generators, Nature 536 (2016) 197–200.
[16] L. Cao, F. Xiao, Y. Feng, W. Zhu, W. Geng, J. Yang, et al., Anomalous Channel-length dependence in nanofluidic osmotic energy conversion, Adv. Funct. Mater. 27 (2017).
[17] R. Long, Z. Kuang, Z. Liu, W. Liu, Temperature regulated reverse electrodialysis in charged nanopores, J. Membr. Sci. 561 (2018) 1–9.
[18] R. Long, F. Wu, X. Chen, Z. Liu, W. Liu, Temperature-depended ion concentration polarization in electrokinetic energy conversion, Int. J. Heat Mass Tran. 168 (2021).
[19] X. Zhang, Z. Qu, Q. Wang, M. Iqbal, Geometry design and mechanism analysis of artificial nanoroughness for enhanced osmotic energy conversion, Energy Convers. Manag. 273 (2022), 116373.
[20] S. Tseng, Y.M. Li, C.Y. Lin, J.P. Hsu, Salinity gradient power: influences of temperature and nanopore size, Nanoscale 8 (2016) 2350–2357.
[21] Y. Hu, Y. Teng, Y. Sun, P. Liu, L. Fu, L. Yang, et al., Bioinspired poly (ionic liquid) membrane for efficient salinity gradient energy harvesting: electrostatic crosslinking induced hierarchical nanoporous network, Nano Energy 97 (2022).
[22] Q. Ren, Q. Cui, K. Chen, J. Xie, P. Wang, Salinity-gradient power harvesting using osmotic energy conversion with designed interfacial nanostructures under thermal modulation, Desalination 535 (2022).
[23] Z. Zhang, P. Zhang, S. Yang, T. Zhang, M. Loffler, H. Shi, et al., Oxidation promoted osmotic energy conversion in black phosphorus membranes, Proc. Natl. Acad. Sci. U. S. A. 117 (2020) 13959–13966.
[24] Z. Zhang, S. Yang, P. Zhang, J. Zhang, G. Chen, X. Feng, Mechanically strong MXene/Kevlar nanofiber composite membranes as high-performance nanofluidic osmotic power generators, Nat. Commun. 10 (2019) 2920.
[25] W. Xin, L. Jiang, L. Wen, Two-dimensional nanofluidic membranes toward harvesting salinity gradient power, Acc. Chem. Res. 54 (2021) 4154–4165.
[26] R. Li, J. Jiang, Q. Liu, Z. Xie, J. Zhai, Hybrid nanochannel membrane based on polymer/MOF for high-performance salinity gradient power generation, Nano Energy 53 (2018) 643–649.
[27] R. Long, M. Li, X. Chen, Z. Liu, W. Liu, Synergy analysis for ion selectivity in nanofluidic salinity gradient energy harvesting, Int. J. Heat Mass Tran. 171 (2021), 121126.
[28] M. Graf, M. Lihter, D. Unuchek, A. Sarathy, J.-P. Leburton, A. Kis, et al., Light-Enhanced blue energy generation using MoS2 nanopores, Joule 3 (2019) 1549–1564.
[29] Q. Wang, Z. Qu, X. Zhang, L. Chen, Electronic-level insight into interfacial effects and their induced anisotropic ion diffusion and ion selectivity in nanochannels, ACS Appl. Mater. Interfaces 14 (2022) 37608–37619.
[30] X.F. Zhang, X. Zhang, Z.G. Qu, J.Q. Pu, Q. Wang, Thermal-enhanced nanofluidic osmotic energy conversion with the interfacial photothermal method, Appl. Energy 326 (2022), 120005.
[31] R. Long, Z. Kuang, Z. Liu, W. Liu, Ionic thermal up-diffusion in nanofluidic salinity-gradient energy harvesting, Natl. Sci. Rev. 6 (2019) 1266–1273.
[32] R. Long, Z. Luo, Z. Kuang, Z. Liu, W. Liu, Effects of heat transfer and the membrane thermal conductivity on the thermally nanofluidic salinity gradient energy conversion, Nano Energy (2019), 104284.
[33] T. Badessa, V. Shaposhnik, The electrodialysis of electrolyte solutions of multi-charged cations, J. Membr. Sci. 498 (2016) 86–93.
[34] D.A. Vermaas, J. Veerman, M. Saakes, K. Nijmeijer, Influence of multivalent ions on renewable energy generation in reverse electrodialysis, Energy Environ. Sci. 7 (2014) 1434–1445.
[35] T. Rijnaarts, E. Huerta, W. van Baak, K. Nijmeijer, Effect of divalent cations on RED performance and cation exchange membrane selection to enhance power densities, Environ. Sci. Technol. 51 (2017) 13028–13035.
[36] D. Pintossi, C.-L. Chen, M. Saakes, K. Nijmeijer, Z. Borneman, Influence of sulfate on anion exchange membranes in reverse electrodialysis, npj Clean Water 3 (2020) 1–10.
[37] J.W. Post, H.V.M. Hamelers, C.J.N. Buisman, Influence of multivalent ions on power production from mixing salt and fresh water with a reverse electrodialysis system, J. Membr. Sci. 330 (2009) 65–72.
[38] E. Guler, W. van Baak, M. Saakes, K. Nijmeijer, Monovalent-ion-selective membranes for reverse electrodialysis, J. Membr. Sci. 455 (2014) 254–270.
[39] M. Abdollahzadeh, M. Chai, E. Hosseini, M. Zakertabrizi, M. Mohammad, H. Ahmadi, et al., Designing angstrom-scale asymmetric MOF-on-MOF cavities for high monovalent ion selectivity, Adv. Mater. 34 (2022) 2107878.

[40] J. Moreno, V. Diez, M. Saakes, K. Nijmeijer, Mitigation of the effects of multivalent ion transport in reverse electrodialysis, J. Membr. Sci. 550 (2018) 155–162.
[41] D. Pintossi, C. Simoes, M. Saakes, Z. Borneman, K. Nijmeijer, Predicting reverse electrodialysis performance in the presence of divalent ions for renewable energy generation, Energy Convers. Manag. 243 (2021), 114369.
[42] X. Chen, Z. Luo, R. Long, Z. Liu, W. Liu, Impacts of transmembrane pH gradient on nanofluidic salinity gradient energy conversion, Renew. Energy 187 (2022) 440–449.
[43] S. Tseng, Y.-R. Hsu, J.-P. Hsu, Diffusiophoresis of polyelectrolytes: effects of temperature, pH, type of ionic species and bulk concentration, J. Colloid Interface Sci. 459 (2015) 167–174.
[44] S. Das, A. Guha, S.K. Mitra, Exploring new scaling regimes for streaming potential and electroviscous effects in a nanocapillary with overlapping Electric Double Layers, Anal. Chim. Acta 804 (2013) 159–166.
[45] J.J. Lopez-Garcia, J. Horno, C. Grosse, Transport properties in nanochannels: ionic size-, permittivity-, and viscosity-related effects, J. Phys. Chem. C 124 (2020) 10764–10775.
[46] J.J. Lopez-Garcia, J. Horno, C. Grosse, Diffuse double-layer structure in mixed electrolytes considering ions as dielectric spheres, The European Physical Journal E 41 (2018) 102.
[47] J.J. Lopez-Garcia, J. Horno, C. Grosse, Ionic size, permittivity, and viscosity-related effects on the electrophoretic mobility: a modified electrokinetic model, Physical Review Fluids 4 (2019), 103702.
[48] G. Mansoori, N.F. Carnahan, K. Starling, T. Leland Jr., Equilibrium thermodynamic properties of the mixture of hard spheres, J. Chem. Phys. 54 (1971) 1523–1525.
[49] T. Boublik, Hard-sphere equation of state, J. Chem. Phys. 53 (1970) 471–472.
[50] L. Cao, F. Xiao, Y. Feng, W. Zhu, W. Geng, J. Yang, et al., Anomalous Channel-length dependence in nanofluidic osmotic energy conversion, Adv. Funct. Mater. 27 (2017), 1604302.